AIAA 2012-4875

High-Performance Computing for Optimal Disruption of Hazardous NEOs

Brian D. Kaplinger* and Bong Wie†
Iowa State University, Ames, IA, 50011, United States

This paper is concerned with the problem of developing high-performance computing approaches for optimal disruption analysis and design of near-Earth objects (NEOs). Past models of a hypervelocity impact fragmentation of an NEO are addressed, and applied to a 3D inhomogeneous asteroid model with randomly generated sections and material parameters. The effects of uncertainty in modeling behavior are examined for a penetrating explosive mission with a two-body spacecraft. Optimization of mission effectiveness design for this type of mission is discussed, with suggestions for a comparison in efficacy. The effects of the target orbit are analyzed by creating a parameterization in (a, e, i) space, sampled from statistics of the known NEO distribution. Characteristics of impacting orbits in this space are introduced, with correlations to the uncertainties in orbital tracking.

Nomenclature

a	semi-major axis
e	eccentricity
i	inclination
a_t	EOS parameter, linear density coefficient
b_t	EOS parameter, hyperbolic density coefficient
A_t	EOS parameter, linear compression coefficient
B_t	EOS parameter, quadratic compression coefficient
α_t	EOS parameter, linear exponent coefficient
β_t	EOS parameter, quadratic exponent coefficient
E_O	EOS parameter, nominal specific energy
E_{iv}	EOS parameter, specific energy of initial vaporization
E_{cv}	EOS parameter, specific energy of complete vaporization
$S^{\alpha\beta}$	deviatoric stress tensor
$R^{\alpha\beta}$	rotation rate tensor
$\epsilon^{\alpha\beta}$	strain rate tensor
$\sigma^{\alpha\beta}$	local strain tensor
$D^{\alpha\beta}$	local strain tensor
σ^{ν}	scalar directional strain magnitude
$\Lambda^{\alpha\nu}$	tensor strain eigenvectors
Δ^{ν}	scalar directional damage
$D^{\max}$	maximum directional damage
n	number of active material flaws

*Research Assistant, Department of Aerospace Engineering, AIAA Student Member.
†Vance Coffman Endowed Chair Professor, Department of Aerospace Engineering, AIAA Associate Fellow

n^{tot}	total nodal flaws
ϵ^{act}	flaw strain activation
G_s	shear modulus
x_E	x coordinate for Earth
y_E	y coordinate for Earth
z_E	z coordinate for Earth
h	specific angular momentum
μ	solar gravitational parameter
r	orbit scalar distance
v	orbit velocity magnitude
θ	true anomaly
v_r	orbit radial velocity

I. Introduction

THE threat of a hazardous asteroid impacting the Earth is a subject that has garnered much attention over the past couple decades. One of the issues that remain unresolved is the engineering of systems capable of deflecting or disrupting these threats. Further, large asteroids on impacting trajectories have yet to be identified. Therefore, it is unknown whether a proposed system could reach a majority of orbits for these types of objects within a reasonable timeframe, while controlling mission parameters such as the relative approach velocity. It has been shown that disruption of a small body can be a viable late-term mitigation method for a variety of orbits [1], with a small set of possible break-up behaviors of the target. The current project extends this exploration to asymmetric and 3D targets, in an effort to better characterize the orbits for which this approach may yield satisfactory results.

The problem to be solved is that of a disrupted NEO dispersing along the orbit as a result of a standoff, contact, or subsurface nuclear explosion mission. Initial simulations in [1, 2] used a spherical axisymmetric NEO model, with the key limitations being the size of the target and a lack of a range of source energy input. With a new computational approach to the hydrodynamic simulations, we efficiently compute results for a 3D shape of general characteristics. This will allow the current model to address much larger targets with increased resolution and a faster turnaround time, so the influence of more parameters can be investigated. A nonlinear orbit solver is presented that calculates an impacting trajectory given boundaries of a (a, e, i) sampling space. This approach increases our understanding of what components of the interplanetary environment affect the likelihood of an NEO being on a collision path with the Earth. Dispersion along these orbits is computed to determine mission effectiveness for a variety of possible cases.

New high-throughput neighbor-finding methods are suggested for the particle representation of disrupted NEOs. This approach becomes more effective using the GPU acceleration technology of the current simulation toolkit. In contrast to the Weibull distribution used to seed implicit flaws in brittle materials [1, 2], the current simulation set develops a tensor relationship for material characteristics and orientation. This allows for more realistic size and shape generation for NEO fragments by treating damage as a local quantity (cracks) rather than a distributed state variable. GPU acceleration of this model is up to 200x on a single workstation, continuing a trend of increasing computational complexity while also increasing efficiency. This approach allows us to compute a range of values rather than monolithic single simulations, and is incredibly important for the orbital analysis. Sensitivity to the orbital parameters is a true unknown, since large impacting NEOs have yet to be observed, so computation for a range of these values is a necessity.

Previous work [2, 3] showed that a large amount of data can be processed using GPU simula-

tion. Initial work was focused mostly on prediction of relative impacting mass, but disruption at different times along a given orbit can have a large effect on the resulting shape of debris. The proposed approach looks at the fragmentation model to better address how uncertainty in the NEO breakup affects orbital prediction, particularly in the case of variable time-to-impact. This allows for a more clear set of objectives for mission design. Another new result is the availability of representative 3D fragment distributions for non-spherical bodies. This will improve the trajectory of the desired hypervelocity intercept mission by allowing full degrees of freedom in choosing the approach asymptote.

II. Target Model

The nominal asymmetric target consists of a contact binary system with a rubble pile exterior. With binary systems comprising about 16% of the known NEA population [4], an impactor mission faces an approximately 1 in 6 chance that the target it approaches will be a binary system. This is a characteristic that will be unable to be predicted ahead of time without radar observation, in the case of systems with close secondaries. It has been suggested that many irregularly shaped asteroids with unusual spin states could be contact binary (or multiple) systems. These types of systems would exhibit some of the same characteristics as monolithic rocks and as rubble piles [5]. Further, those asteroids identified as rubble piles could have large solid components beneath their regolith.

The two cores of the model system are elliptical, with major and minor axes of 50 and 30 meters, respectively. These cores are given material properties similar to granite using a linear elastic-plastic strength model, are canted by 45 degrees relative to the horizontal. There is a vertical line of symmetry, so the cores are mirror images of one another. A rubble regolith extends 2 meters in depth vertically above each core, and is packed along lines of constant potential around the body, resulting in a maximum regolith depth of 14 meters. These properties result in exterior dimensions of the target being approximately 76 x 42 meters, as shown in Figure 1. The inner half of each core has an initial bulk density of 2630 kg/m^3, while the outer portion of the core is more porous material with an average bulk density of 1910 kg/m3. Both sections use values for yield strength between 7-203 MPa and shear modulus between 8-22 MPa. For the impactor portion of the mission, the Tillotson equation of state is used, with the parameters listed in Table 1.

Table 1. Parameters for Tillotson Equation of State in Core Material

Parameter	Numerical Value	Units
a_t	0.5	
b_t	1.5	
A_t	7.1E10	Pa
B_t	7.5E10	Pa
α_t	5	
β_t	5	
E_0	4.87E8	J/kg
E_{iv}	4.72E6	J/kg
E_{cv}	1.82E7	J/kg

The initial impactor of the two-body spacecraft is an aluminum wedge 1 m in base diameter and 1.5 m in length. The nuclear payload follows, depositing 70 kilotons of energy upon reaching the initial impact site of the lead body. Most of this energy is absorbed in the crater region formed by the initial impact, though deeper absorption is allowed due to the fact that much of the material

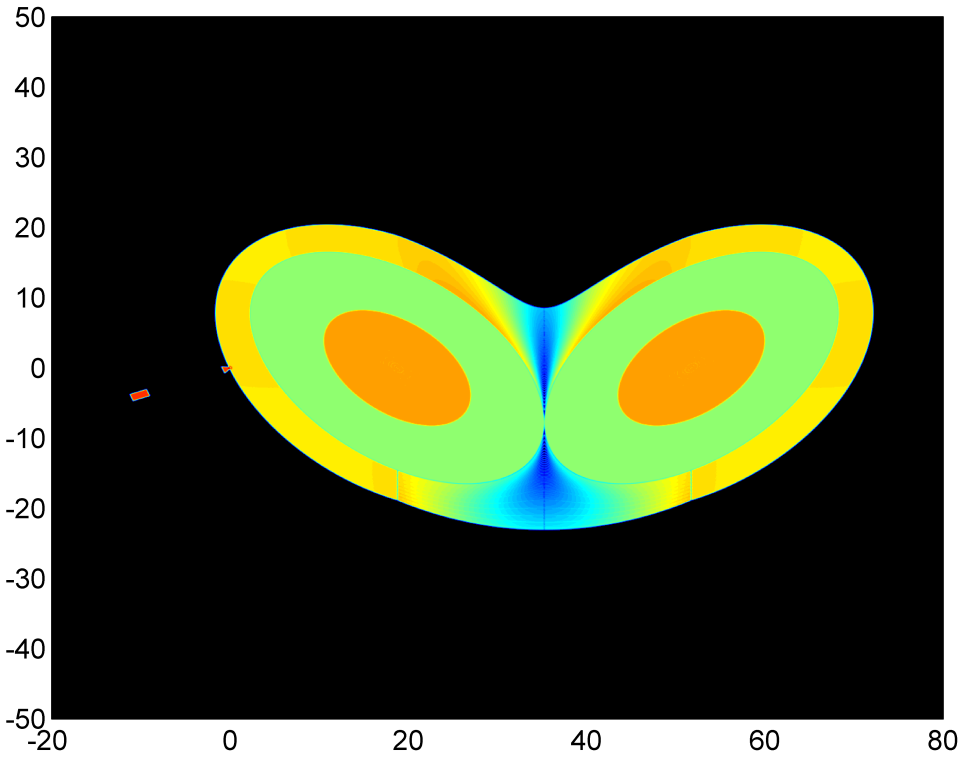

Figure 1. Asymmetric Target for 3D Penetrated Explosive Modeling.

in this region has already been vaporized and superheated into a plasma state. The resulting shock wave has a peak compression of more than 2 times the initial density, and quickly overtakes the initial shock of the lead body impact, which is much weaker. This shock compresses much of one core far beyond the fracture strength of even the worst case material, rebounding off of the nearer side. This asymmetric behavior dissipates some energy due to interactions with the rebounding shock front. In the center area of deeper regolith, the seeding process naturally results in a much more porous material, absorbing energy from the shock. Upon reaching the second core at the far side, some large chunks escape the disruption process in some cases (even with lower material strengths).

In addition to the equations of motion used for the previous simulation version [1], an extra dimension was added. This was to investigate the potential for sources of errors in 2D cylindrical Smoothed Particle Hydrodynamics (SPH) codes, rather than an axisymmetric model. Other than in increase to the complexity of neighbor-finding calculations (as discussed later), no significant increase in code complexity was required. This is due to the fact that the SPH model equations are originally a 3D component/tensor formulation.

A. Tensor Damage Model

In the initial SPH model for comparison, the behavior of the core material under high stress is governed by the activation of implicit flaws. These flaws are seeded in the representation particles using a Weibull distribution with a coefficient of around 4.2E23 and an exponent between 6.2-9.5. Using a range of distribution exponents and strength properties allows us to examine the behavior of the core material with varying brittleness and material cohesion. This turns out to be very important for this contact binary system, as strong core material absorbs energy from the disruption shock and can result in large remaining chunks of material. Smoothing lengths are

chosen to allow for resolution of between 1 cm and 5 cm, which results in a hydrodynamic system of between 800,000 and 6,000,000 nodes. This system is scaled to be an ideal size for the GPU simulation programs developed at the Iowa State Asteroid Deflection Research Center (ADRC), maximizing both computational efficiency and simulation turnaround time.

For this comparison, a damage model using a tensor variable was implemented. The details are the same as those used in the Spheral code, developed by Mike Owen at the Lawrence Livermore National Laboratory. The variable tracked for material stress is the deviatoric stress tensor, $S^{\alpha\beta}$, which is advanced using a modification of Hooke's law [6,7]:

$$\frac{DS_i^{\alpha\beta}}{Dt} = 2G_s\left(\epsilon_i^{\alpha\beta} - 3\delta_i^{\alpha\beta}\epsilon_i^{\gamma\gamma}\right) + S_i^{\alpha\gamma}R_i^{\beta\gamma} + R_i^{\alpha\gamma}S_i^{\gamma\beta} \tag{1}$$

where $R^{\alpha\beta}$ is the local rotation rate tensor, $\epsilon^{\alpha\beta}$ is the local strain rate tensor, G_s is the shear modulus, and the SPH approximation for these terms is given by

$$\epsilon_i^{\alpha\beta} = \frac{1}{2}\sum_{j=1}^{N}\frac{m_j}{\rho_j}\left[(v_j^\alpha - v_i^\alpha)\frac{\partial W(\mathbf{x}_j - \mathbf{x}_i)}{\partial x^\beta} + (v_j^\beta - v_i^\beta)\frac{\partial W(\mathbf{x}_j - \mathbf{x}_i)}{\partial x^\alpha}\right] \tag{2}$$

$$R_i^{\alpha\beta} = \frac{1}{2}\sum_{j=1}^{N}\frac{m_j}{\rho_j}\left[(v_j^\alpha - v_i^\alpha)\frac{\partial W(\mathbf{x}_j - \mathbf{x}_i)}{\partial x^\beta} - (v_j^\beta - v_i^\beta)\frac{\partial W(\mathbf{x}_j - \mathbf{x}_i)}{\partial x^\alpha}\right] \tag{3}$$

We use a tensor damage variable defined per node $D^{\alpha\beta}$ in order to support directionality in the damage evolution. Cracks are allowed to open up in response to strain aligned perpendicularly to that direction, there is substantially reduced crack growth in orthogonal directions to the strain. The tensor strain, $\sigma^{\alpha\beta}$ used is the "pseudo plastic strain" of SolidSpheral, due to Mike Owen, which evolves in time as

$$\frac{D\sigma_i^{\alpha\beta}}{Dt} = \frac{1}{G_s}\frac{DS_i^{\alpha\beta}}{Dt} \tag{4}$$

This is decomposed into a set of eigenvalues, σ^ν, and eigenvectors, $\Lambda^{\alpha\nu}$, from which the directional scalar damage, Δ^ν is the magnitude of the ν-th column of $D^{\alpha\gamma}\Lambda^{\gamma\beta}$. The maximum damage allowed to accumulate in a volume, similar to the formulation in [1, 2] but allowing for directionality, is:

$$D^{\max} = \max\left(\frac{n_i}{n_i^{\text{tot}}}, \Delta_i^\nu\right) \tag{5}$$

where n_i is the number of active flaws ($\epsilon > \epsilon^{\text{act}}$) and n^{tot} is the total number of flaws assigned to a particle, which can vary widely, but is always at least one. These directional damages can then be time evolved using representative scalar evolution laws [1,8].

B. Neighbor Finding Implementation

One of the key limitations of past simulation approaches is that most proposed neighbor-finding methods for interpolation rely on complex logic and lists not suitable for efficient GPU implementation. Therefore, the addition of the third dimension makes this problem far more complex. A new approach for efficiently computing unions and intersections of integer sets on the GPU is proposed, allowing for neighbor-finding as an update process from previously computed relative relationships. Based on a standard Sort-and-Sweep approach in computer graphics [9], the power of this approach lies in how it scales with increased number of SPH interpolants. In addition to

scaling superlinearly (compared to quadratic brute force calculations), the present approach uses the Thrust library to sort the position components of the particles in parallel. This eliminates a series of memory transfers with the host and keeps all data on the GPUs.

A subsequent group of GPU kernels establish pointers to the limits on the sorted array for which candidate neighbor particles may belong. This reduces the neighbor finding to an integer union calculation, which can be conducted as a logical (true/false) operation. Comparing the position of the sorted particle IDs with the limits allows for a simple yes/no decision on whether a proposed neighbor could be within the support of the interpolation function. Figure 2 gives a depiction of this process for each computing thread. Figure 3 shows the improvements of the present model over in-place neighbor calculations (also on the GPU). While dimensionality affects the speed-up, there are still substantial gains made over past implementations.

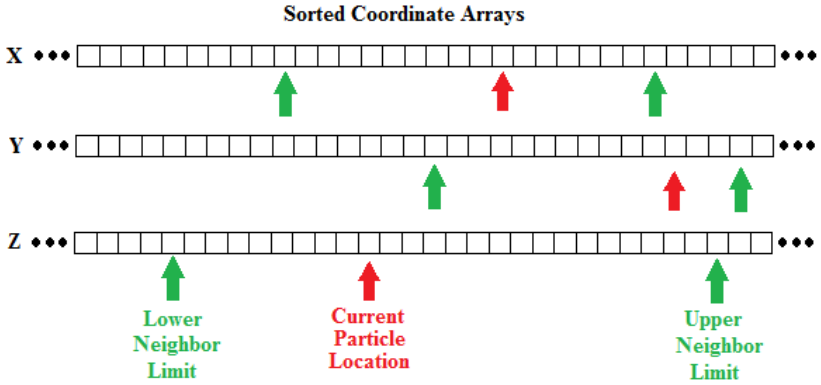

Figure 2. Description of Sorted Neighbor Kernel Process.

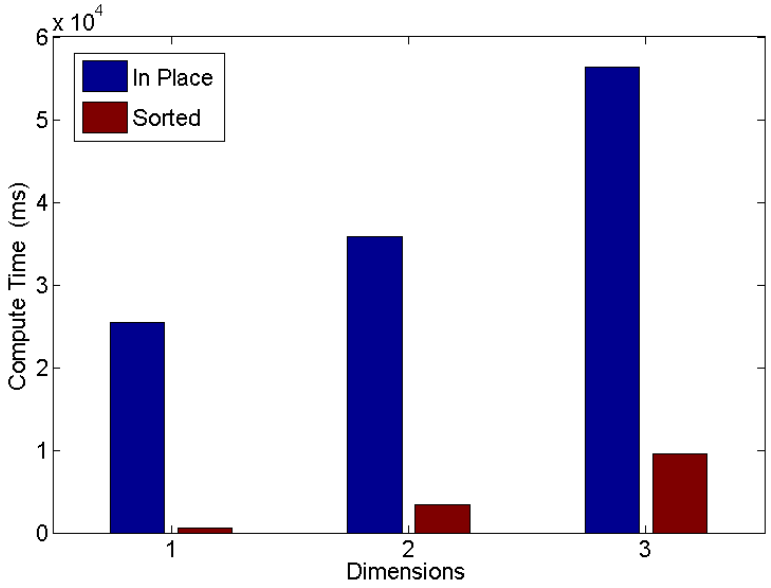

Figure 3. Neighbor Search Cost.

III. Orbit Model

This part describes the identification of nominal orbits for a fixed impact time. Given a desired lead time, the optimal approach vector is computed using a differential step update, described in the following subsections. The cost parameter is the impacting percentage of the original target mass.

A. Impacting Orbit Solver

The orbital parameters for the nominal trajectory are sampled from a (a, e, i) space that represents the distribution of known NEOs, as shown in Figure 4. This is done using inverse transform sampling, in which a random number is mapped to the integral of the cumulative density function for each of these three parameters. Given a, e, i, and the impact date, we have all of the information needed to pin down an impacting orbit. If we assume that the orbit passes through the center of the Earth, then we have x_E, y_E, and z_E, which are the Cartesian coordinates for the Earth's center of mass at that epoch, which coincide with a point on the desired orbit.

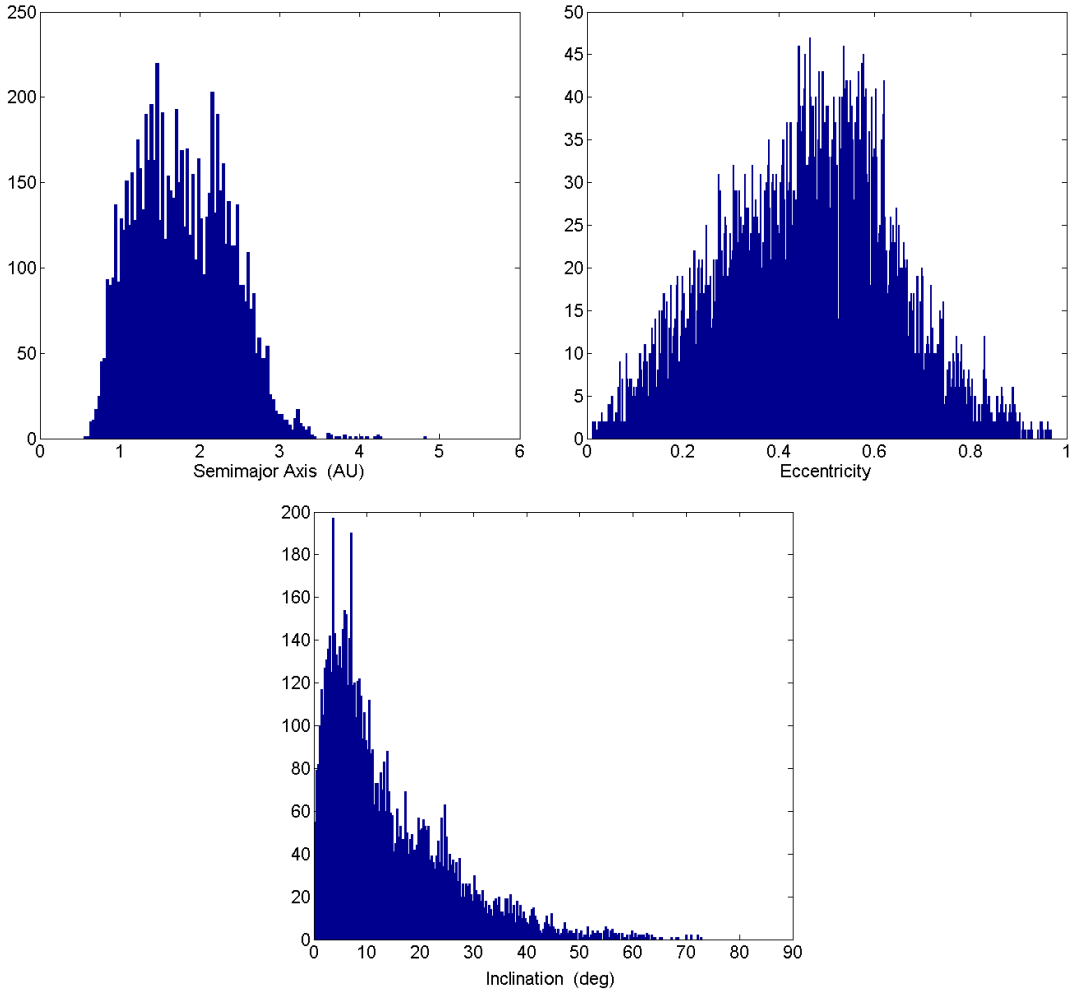

Figure 4. Histograms of Known NEO Population.

Given a, e, and $r = \sqrt{x_E^2 + y_E^2 + z_E^2}$, the specific angular momentum is calculated as $h = \sqrt{\mu a(1-e^2)}$ [10,11]. Then, the true anomaly, θ and velocity magnitude, v, are calculated using

the orbit equation and the vis-viva equation:

$$r = \frac{h^2}{\mu}\frac{1}{1+e\cos\theta}; \qquad \frac{v^2}{2} - \frac{\mu}{r} = -\frac{\mu}{2a} \tag{6}$$

We can also calculate the radial velocity, v_r, as

$$v_r = \frac{\mu}{h} e \sin\theta \tag{7}$$

which gives us all the needed scalars to solve the following set of nonlinear equations for the velocity components v_x, v_y, and v_z, resulting in the desired state vector:

$$\begin{aligned} f_1(v_x, v_y, v_z) &= 0 = xv_y - yv_x - h\cos i \\ f_2(v_x, v_y, v_z) &= 0 = xv_x + yv_y + zv_z - rv_r \\ f_3(v_x, v_y, v_z) &= 0 = \sqrt{v_x^2 + v_y^2 + v_z^2} - v \end{aligned} \tag{8}$$

B. Mission Approach Asymptotes

Statistics representing the fragmented system are collected and stored as cumulative density functions for the needed variables, similar to those shown in [1]. A representative fragment system of 10,000 to 100,000 fragments is created from these statistics using inverse transform sampling. The debris cloud is given global coordinates in a Local-Vertical-Local-Horizontal (LVLH) reference frame about the center of mass. Since the LVLH reference frame is computationally beneficial for self-gravity and collision modelling among fragments [3], we use the nonlinear relative equations of motion for this frame to govern fragment trajectories [10,11]. Because the hydrodynamic model has a definite direction of maximum momentum along the initial approach asymptote, a desired deflection direction must be chosen.

Given a fixed lead time in which to allow the fragmented target to disperse along its orbit, or even a minimal desired lead time, we have a point (or set) at which a desired intercept is acheived. It is clear, however, that not all approach vectors are equal. From a mission design perspective, the approach asymptote affects the transfer orbit, and therefore the cost (or even feasibility) of the mission [12]. For the present study, bounds on the approach asymptote from a mission perspective are not considered. Rather, the direction in which the approach occurs is a deciding factor in the behavior of the fragmenting body. Past work has shown that there is a clear bias towards dispersion along this vector for most of the tested hydrodynamic simulations [1].

A simple differential optimization routine is applied to this vector for each of the sampled impacting orbits. There are two degrees of freedoms for each of these problems. The optimal pointing direction will be something of interest in short warning scenarios, since a drastic difference in the dispersion patterns can occur. For some of the orbits, a grid search of the approach asymptotes was done to quantify the range of impacting mass ratios.

IV. Computational Approach

A. Energy Source Comparison

The first target is a rubble-pile asteroid, with a bulk density of 1.91 g/cm^3. This is a likely target for demonstrating the behavior of more porous material. The second target contains granite boulders at the elliptical cores with a bulk density of 2.63 g/cm^3. A linear model for material strength is used in this target with a yield strength of 14.6 MPa and a shear modulus of 35 MPa, resulting in a more

granulated fragmentation and slower dispersion velocities. Real asteroid targets are expected to fall within these two extremes, with variances for composition, distribution of mass, and orientation.

We use the Tillotson equation of state [13] in the solid asteroid and in the aluminum penetrator used to deliver the surface explosive. This is modified to include porosity, and an irreversible crush strength, for the rubble pile target [14,15]. We assume a power law distribution for number of implicit flaws in a volume of material with respect to local tensile strain, and assign flaws with specific activation thresholds to each SPH particle [8]. These flaws are then fed into the previously discussed damage model.

The initial conditions for all three methods of NEO deflection using nuclear explosive devices include an energy source of 80 kt. Thermal emission is omitted from the subsurface and surface explosions due to absorption by surrounding material in the time scale of interest. For the subsurface case, the explosive is modeled as a cylindrical energy source buried at a depth of 5 meters. The blast wave compresses the NEO, reducing it to fragments, and disperses it primarily along the axis of the explosion. The resulting fragment distribution for a case like this has a peak between 20-70 m/s, with a tail of high-speed ejecta. The second model, includes an aluminum penetrator impacting the surface at 10 km/s. The explosion thermal energy turns the high-mass impactor into a plasma, which burrows into the surface as it releases its energy. Slower dispersion velocity is observed than the subsurface case, but this approach is extremely beneficial from an engineering standpoint, as there is strong coupling between time-to-impact and a reduction in mission fuel cost [12]. The benefit to this method relative to a subsurface explosion is that it does not require a rendezvous, and therefore there are available launch windows for this type of mission right up until immediately before the impact date.

For a standoff blast, additional physics must be considered. An energy deposition strategy is required that does not directly compute X-ray and neutron scattering in the target. For this, a raytracing algorithm is used, as outlined in [1]. A 10% neutron yield is assumed for these simulations, and a maximum deposition depth of 1.5 m to compare to deposition predicted for chondritic materials. A modified SPH node representation is created that resembles an ablative modeling grid used in high-energy deposition physics. This distribution is shown in Fig. 6, and has a minimum smoothing scale of 0.1 cm with a maximum local change rate of 10% up to 0.2 m resolution.

B. GPU Implementation

This section address the computational approach used to solve the disruption problem. Each state variable update for a fragment is conducted in parallel at each time step. Each thread on the GPU calculates the state variable change for one fragment, with the GPU kernel limited to one time step. This is necessary because the positions of the planets and other gravitating bodies must be calculated and transferred to the GPU at each time step. Additionally, the positions of fragments at each integration substep are shared among multiple GPUs and CPU threads. For this reason, the present hydrodynamics model is predominantly bandwidth-limited for small data sets.

We retain the information for neighbors connected by material strength, as well as carrying neighbor information through the correction step of the integrator. This results in a 28% performance improvement over recalculating neighbors at both the prediction and correction steps, while allowing for a variable time step based on the Courant condition, as discussed in [1,2]. While the reduction operation to determine the new time step can be done in parallel, all GPU threads must have position information for all particles to determine neighbors. This requirement could be eliminated through clever domain decomposition, but there is a tradeoff between associating a mesh to the model and taking advantage of contiguous memory sections of particles. Load balancing would also require additional communication between GPUs, which has an impact on performance, as

PCI-E bandwidth is one of the limiting factors in GPU acceleration.

Our memory model for this simulation includes a shared host memory, distributed device memory for each GPU, and data transfers between them handled through explicit array transfer. Each block of compute threads on the GPU takes the data it needs from the global device memory when the kernel reaches its block. This is an important factor, because the varying compute capabilities have different limitations on this block memory, changing the number of threads that may be used in the calculation. Constants are transferred to all GPU memories implicitly using a pointer to the host constant value. While modern dedicated compute GPUs have a high amount of onboard memory, it usually is far less than system memory. Though it may seem advantageous to calculate parameters for every time step before the start of the simulation, the arrays resulting from this approach are quite large. Each model of GPU has a limited number of memory registers available to each computing block of threads. This is addressed in the present code by utilizing asynchronous data transfers and kernel launches to split the work into streams. This allows the CPU to calculate new parameters needed for the next time step while the GPU is updating the current step.

V. Results

A. Hydrodynamic Fragmentation

A slice of the nominal three-dimensional target was shown in Figure **??**. As an increase in computational burden, it performs moderately less efficiently than the two dimensional model. The overall velocity statistics, which are the governing variables behind successful disruption, are similar to those for the cylindrical case. The histogram for radial dispersion velocities of the fractured particles can be seen in Figure 5.

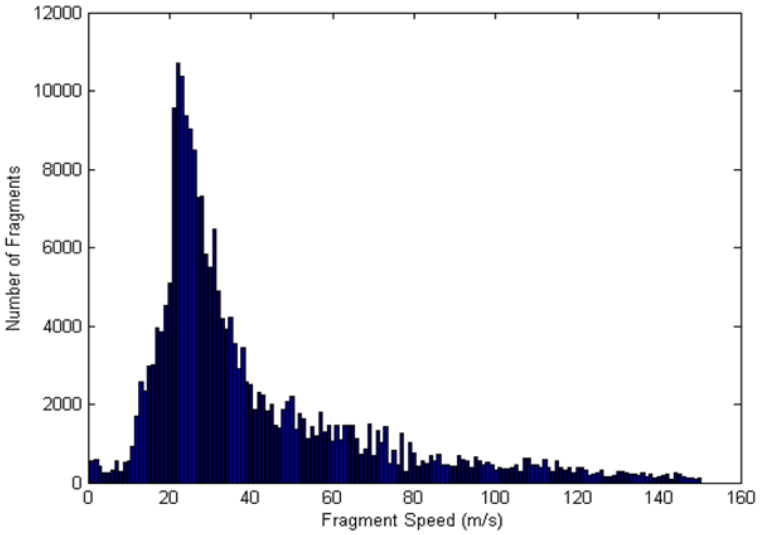

Figure 5. Radial Dispersion Velocity Histogram.

The travel of the explosive shock can be seen in Figure 6. This process dissipates some energy due to interactions with the rebounding shock front. In the center area of deeper regolith, the seeding process naturally results in a much more porous material, absorbing energy from the shock. The new damage model allows for better tracking of crack propagation, such as that shown in Figure 7. Upon reaching the second core at the far side, some large chunks escape the disruption process in some cases (even with lower material strengths). A final hydrodynamic state can be seen in Figure 8.

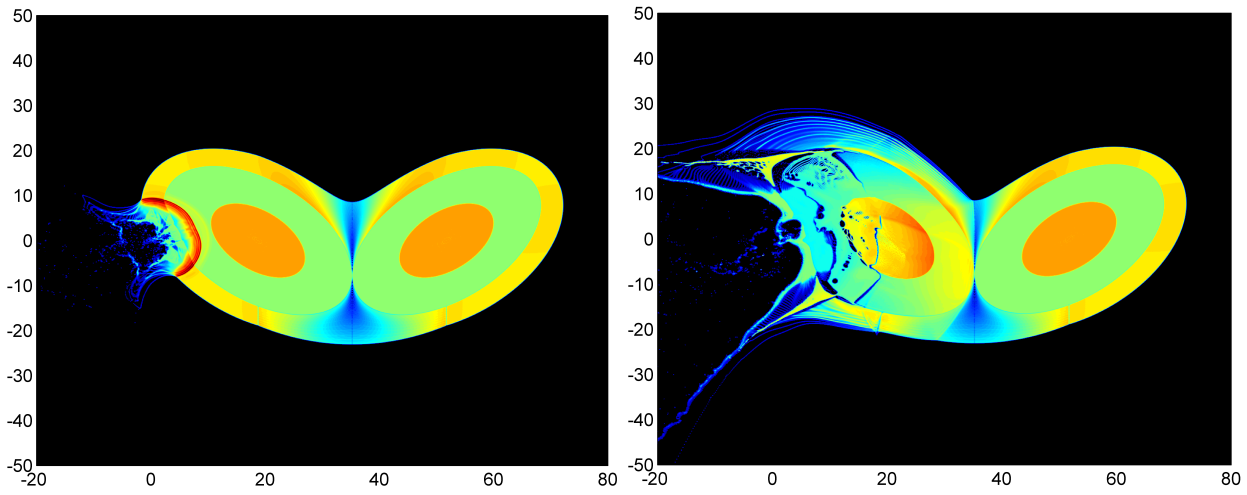

Figure 6. Asymmetric Shock Behavior.

There remains a high risk for this target of single largest chunks on the order of tens of meters. However, this material is highly stressed due to velocity gradients, and may be ripped apart in further time. Further, these large chunks are still imparted substantial velocities from the blast 10-20 m/s, and have sufficient energy to disperse from the nominal impacting trajectory over tens of days.

B. Optimal Mission Results

The present simulation package has the advantage of being able to handle millions of decoupled optimization problems in parallel to one another. Thus, the generation of data outpaces the capability for displaying it in the present work. However, sample results are shown for a nominal impacting trajectory with a lead time of 15 days. Figure 9 shows the cost function contours for approach asymptotes of a sample mission. This impacting trajectory has a semimajor axis of 0.968, an eccentricity of 0.0242, and an inclination of 7.309 degrees.

It is clear for this case that, not only do local optimal solutions exist, but that there are specific conditions which should be avoided. However, this was not the case for all of the virtual impacting trajectories. This fact was especially true for orbits of high eccentricity ($>$ 20 degrees), which had many local minimums, and a wider range of effective dispersion options. Deeper cost function wells existed for these cases, though the geometry was more complicated than the lower inclination case, as shown. The contours are colored according to the base 10 logarithm of the resulting impact probability, showing a range of orders of magnitude. No clear result for the optimal direction for all cases was established. In the sample case, the conditions to be avoided were a perturbation normal to the plane of the orbit. The optimal directions in this case are near parallel to the velocity direction. The vectors forming the solutions of the tested orbits were uniformly distributed, which may be indicative of the lower lead time mission.

As discussed in [12], some approach asymptotes are critical for interception with a single launch. Therefore, future work should address the coupled problem of mission feasibility and mission effectiveness. This will likely place stricter limits on the available lead times and the payload mass deliverable to the target.

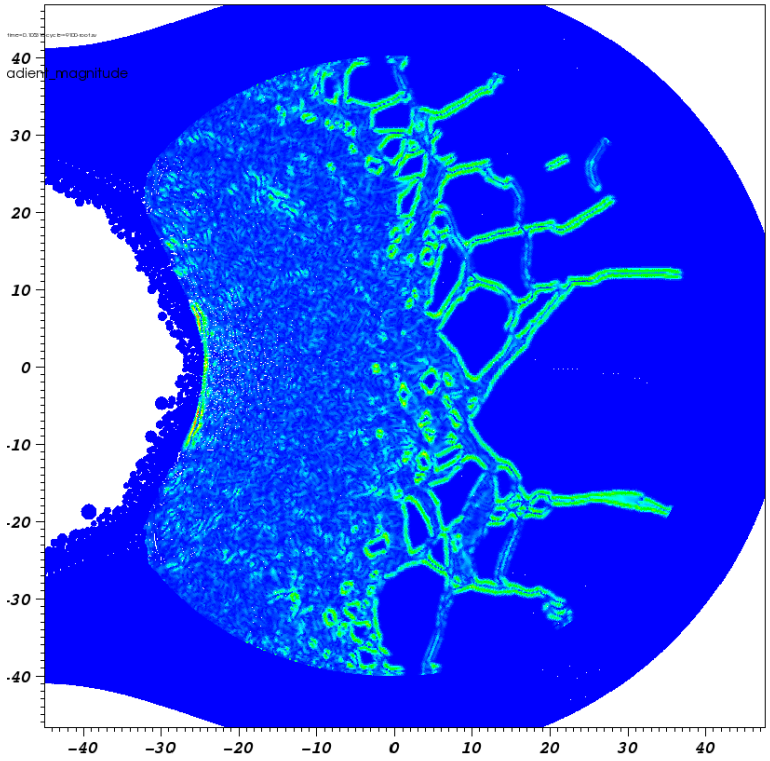

Figure 7. Example Damage Localization for Tensor Fracture Model.

VI. Conclusion

This paper addressed the problem of developing high-performance computing approaches for optimal disruption analysis and design of near-Earth objects. Past models of a hypervelocity impact fragmentation of an NEO were extended and applied to a 3D inhomogeneous asteroid model with randomly generated sections and generic material parameters. A nonlinear orbit solver was presented that calculates an impacting trajectory given boundaries of a (a, e, i) sampling space. Dispersion along these orbits was computed to determine mission effectiveness for a variety of possible cases.

New high-throughput neighbor-finding methods were suggested, using the GPU acceleration technology of the current simulation toolkit. The current simulation set develops a tensor relationship for material characteristics and orientation. This allows for more realistic size and shape generation for NEO fragments by treating damage as a local quantity (cracks) rather than a distributed state variable. GPU acceleration of this model is up to 200x on a single workstation, continuing a trend of increasing computational complexity while also increasing efficiency. This approach allows us to compute a range of values rather than monolithic single simulations, and is incredibly important for the orbital analysis. Sensitivity to the orbital parameters is a true unknown, since large impacting NEOs have yet to be observed, so computation for a range of these values is a necessity.

A large amount of data can be processed using GPU simulation, confirming that disruption at different times along a given orbit can have a large effect on the resulting shape of debris. This allows for a more clear set of objectives for mission design. Another new result is the availability of representative 3D fragment distributions. This will improve the trajectory of the desired hypervelocity intercept mission by allowing full degrees of freedom in choosing the approach asymptote.

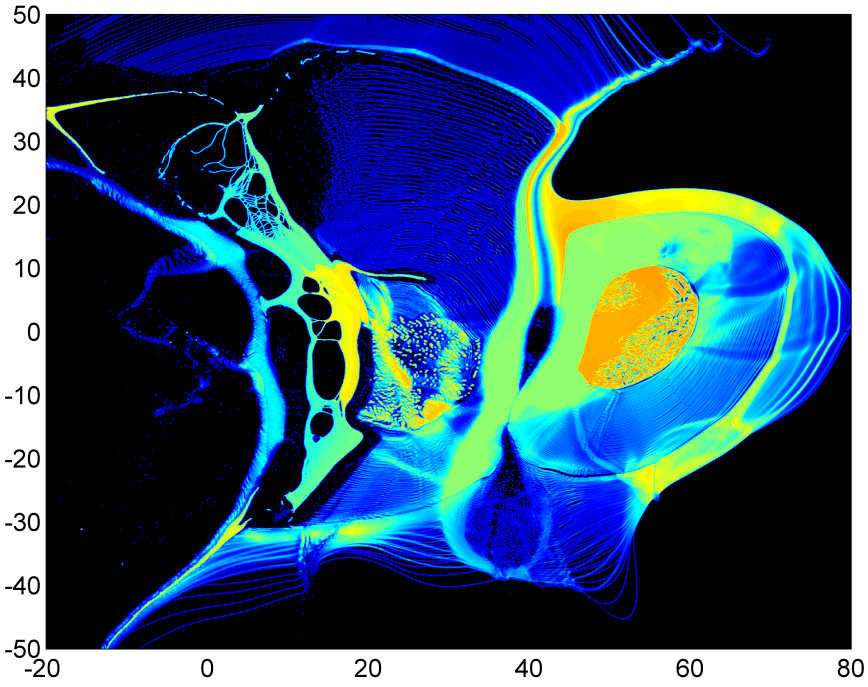

Figure 8. Final Disruption of NEO Target.

Acknowledgments

This research has been supported by the NIAC (NASA Innovative Advanced Concepts) Phase I study project of the NASA Office of the Chief Technologist. The author would like to thank Dr. John (Jay) Falker, the NIAC Program Executive, for his support of this research project. The Authors would like to thank Mike Owen (LLNL) for details on the damage model used in Spheral, as well as for furnishing Figure 8 as an example.

References

[1]Kaplinger, B.D., and Wie, B., "Comparison of Fragmentation/Dispersion Models for Asteroid Nuclear Disruption Mission Design," AAS-11-403, *AIAA/AAS Astrodynamics Specialists Conference*, AAS/AIAA Astrodynamics Specialist Conference, Girdwood, AK, July 31- August 4, 2011.

[2]Kaplinger, B., Wie, B., and Dearborn, D., "Nuclear Fragmentation/Dispersion Modeling and Simulation of Hazardous Near-Earth Objects," IAA-PDC-2138266, *2nd IAA Planetary Defense Conference*, Bucharest, Romania, May 9-12, 2011.

[3]Kaplinger, B., and Wie, B., "Optimized GPU Simulation of a Disrupted Near-Earth Object Including Self-Gravity," AAS-11-266, *21st AAS/AIAA Spaceflight Mechanics Meeting*, New Orleans, LA, February 13-17, 2011.

[4]Margot, J.L., Nolan, M.C., Benner, L.A.M., Ostro, S.J., Jurgens, R.F., Giorgini, J.D., Slade, M.A., Campbell, D.B., "Binary Asteroids in the Near-Earth Object Population," *Science*, 296, 2002.

[5]Michel, P., "Physical Properties of Near-Earth Objects that Inform Mitigation," *2nd IAA Planetary Defense Conference*, Bucharest, Romania, May 9-12, 2011.

[6]Monaghan, J.J, "Smoothed Particle Hydrodynamics," *Rep. on Prog. in Physics*, vol. 68, pp. 1703-1759, July 2005.

[7]Randles, P.W., and Libersky, L.D., "Smoothed Particle Hydrodynamics: Some Recent Improvements and Applications," *Computer Methods in Applied Mechanics and Engineering*, vol. 139, pp. 375-408, 1996.

[8]Benz, W., and Asphaug, E., "Simulations of Brittle Solids using Smooth Particle Hydrodynamics," *Computer Physics Communications*, vol. 87, pp. 253-265, 1995.

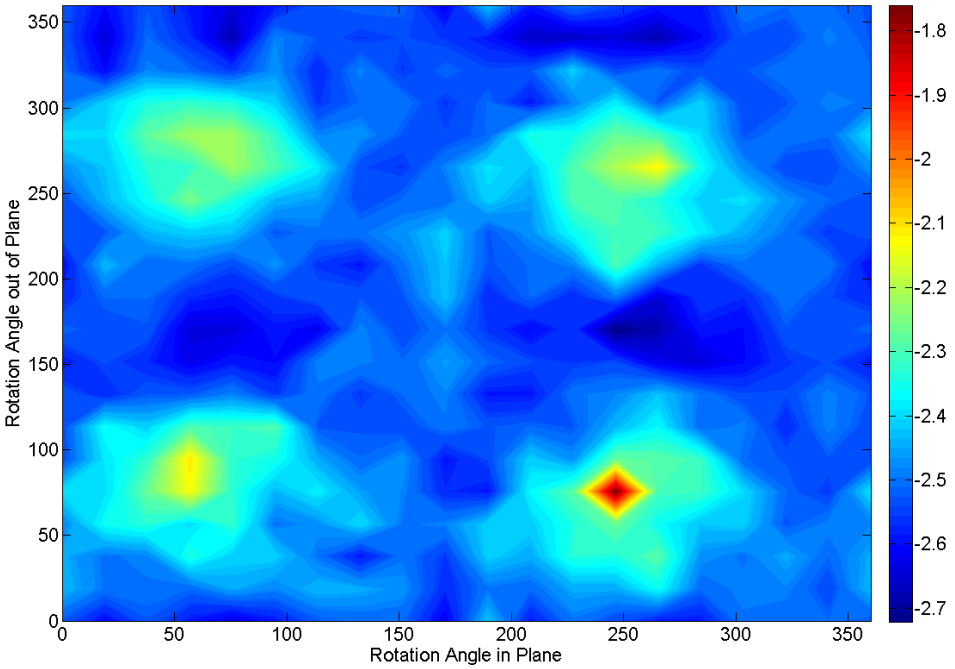

Figure 9. Cost Function Contours for Sample Mission Approach Asymptotes.

[9]LeGrand, S., "Broad-Phase Collision Detection with CUDA," *GPU Gems 3*, ed. H. Nguyen, Addison-Wesley, 2007.

[10]Curtis, H.D., *Orbital Mechanics for Engineering Students*, Elsevier Aerospace Engineering Series, Oxford, UK, 2006.

[11]Vallado, D.A., *Fundamentals of Astrodynamics and Applications*, Third Edition, Microcosm Press, Hawthorne, CA, 2007.

[12]Wagner, S., and Wie, B., "Analysis and Design of Fictive Post-2029 Apophis Intercept Mission for Nuclear Disruption," AIAA-2010-8375, *AIAA/AAS Astrodynamics Specialists Conference*, Toronto, Ontario, Canada, August 2-5, 2010.

[13]Tillotson, J.H., "Metallic Equations of State for Hypervelocity Impact," General Atomic Technical Report GA-3216, 1962.

[14]Jutzi, M., Benz, W., and Michel, P., "Numerical Simulations of Impacts Involving Porous Bodies I. Implementing Sub-Resolution Porosity in a 3D SPH Hydrocode," *Icarus*, vol. 198, pp. 242-255, 2008.

[15]Schuster, S.H., and Isenberg, J. "Equations of State for Geologic Materials," Defense Nuclear Agency Technical Report DNA-2925Z, 1972.